NOAA Technical Memorandum ERL PMEL-57

RECENT OBSERVATIONS OF TIDES AND TIDAL CURRENTS FROM THE NORTHEASTERN BERING SEA SHELF

Harold O. Mofjeld

Pacific Marine Environmental Laboratory
Seattle, Washington
June 1984

UNITED STATES
DEPARTMENT OF COMMERCE

Malcolm Baldrige,
Secretary

NATIONAL OCEANIC AND
ATMOSPHERIC ADMINISTRATION

John V. Byrne,
Administrator

Environmental Research
Laboratories

Vernon E. Derr
Director

NOTICE

Mention of a commercial company or product does not constitute an endorsement by NOAA Environmental Research Laboratories. Use for publicity or advertising purposes of information from this publication concerning proprietary products or the tests of such products is not authorized.

Contribution Number 718 from the Pacific Marine Environmental Laboratory

CONTENTS

		Page
Abstract		1
1.	Introduction	1
2.	Observed Tides	4
3.	Observed Tidal Currents	12
4.	Discussion	22
	4.1 Sverdrup Wave Theory	22
	4.2 Numerical Models	26
5.	Summary	33
6.	Acknowledgements	34
7.	References	35

ABSTRACT

Tide and tidal current observations from the Northeastern Bering Sea Shelf and a comparison of these observations with theory and numerical models are reported in this memorandum. Pressure observations (November 1981 - August 1982) at seven stations show that the diurnal tides dominate the outer shelf. The diurnal amplitudes (maximum of 38 cm for K1 and 26 cm for O1 at the shelfbreak) decrease exponentially inshore from the shelfbreak at a rate consistent with subinertial Sverdrup waves. The phase lags of the diurnal tides vary little (ranging from 322°G to 359°G for the K1 tide) over the shelf. The semidiurnal amplitudes (maximum of 23 cm for M2 at the shelfbreak) change considerably between stations; on the outer shelf there is some influence of a semidiurnal amphidromic system off Cape Navarin. The phase lags of the semidiurnal tides are earliest at the shelfbreak (87°G for M2) and increase toward the east and north (202°G for M2 in Bering Strait and 336°G to the east of St. Lawrence Island). The tides become progressively smaller and semidiurnal toward the north and east from the shelfbreak (an M2 amplitude of 7.7 cm and a K1 amplitude of 2.7 cm in Bering Strait). Non-tidal pressure fluctuations become stronger in the same direction, dominating the pressure signal on the Northern Bering Sea Shelf. There are some seasonal variations in the observed tide and tidal current with slightly larger diurnal tidal amplitudes (increases being ~6% for the K1 tide at the shelfbreak and ~33% for the K1 current in Anadyr Strait) and smaller semidiurnal amplitudes (the strongest decreases being ~18% for the M2 tide in Bering Strait and ~10% for the M2 current in Anadyr Strait) during late winter at some stations. Numerical models reproduce the general features of the observed tides and tidal currents.

1. INTRODUCTION

During November 1981 to August 1982, bottom pressure was recorded at seven stations on the Northeastern Bering Sea Shelf. These stations (Fig. 1) help to fill a major void in the distribution of tide stations on this shelf to the west of St. Matthew and St. Lawrence Islands. The observations were made to provide boundary conditions and interior test points for a three-dimensional numerical model of the combined Bering/Chukchi Sea Shelf under development by Liu and Leenderste (1982, 1984). The time series of bottom pressure (Figs. 2 and 3) have been analyzed for tides, and the resulting tidal harmonic constants form the basis for the first part of this memorandum. The observations also reveal large, non-tidal

fluctuations in bottom pressure away from the shelfbreak which are caused by atmospheric forcing. The non-tidal signal is the subject of future work.

Tidal currents were observed at several stations (Fig. 1) in the same region during November 1980 to June 1981. These and the low- frequency currents are described in Salo, Schumacher, and Coachman (1983). We shall extend their analysis by presenting current harmonic constants and by discussing briefly the tidal dynamics for the outer shelf. Kitani and Kawasaki (1979) observed tidal currents on the outer Bering Sea Shelf and reported diurnal and semidiurnal current ellipses. The general shape and orientations of these ellipses are consistent with those we shall present. The amplitudes of their ellipses are suspect, however, because the current observations were taken using slack-wire moorings with surface floats; such moorings tend to produce anomalously large current speeds.

The tides and tidal currents to the east of St. Matthew and St. Lawrence Islands and on the Southeastern Bering Sea Shelf are described by Pearson, Mofjeld, and Tripp (1981). Some of the tide stations reported in this memorandum are in that region. We include the new tidal observations from these stations for completeness and to consider whether low-frequency variations in the tidal harmonic constants occur simultaneously over the larger region.

The primary source for the tidal energy on the Bering Sea Shelf is the Pacific Ocean with a small contribution from the Arctic Ocean (Harris, 1904; Leonov, 1960; Office of Climatology and Oceanographic Analysis Division, 1961; Defant, 1961; Coachman, Aagaard, and Tripp, 1975; Sündermann, 1977; and Pearson, Mofjeld, and Tripp, 1981). Because the Bering Sea Shelf is so large, it supports complicated patterns of tides and tidal

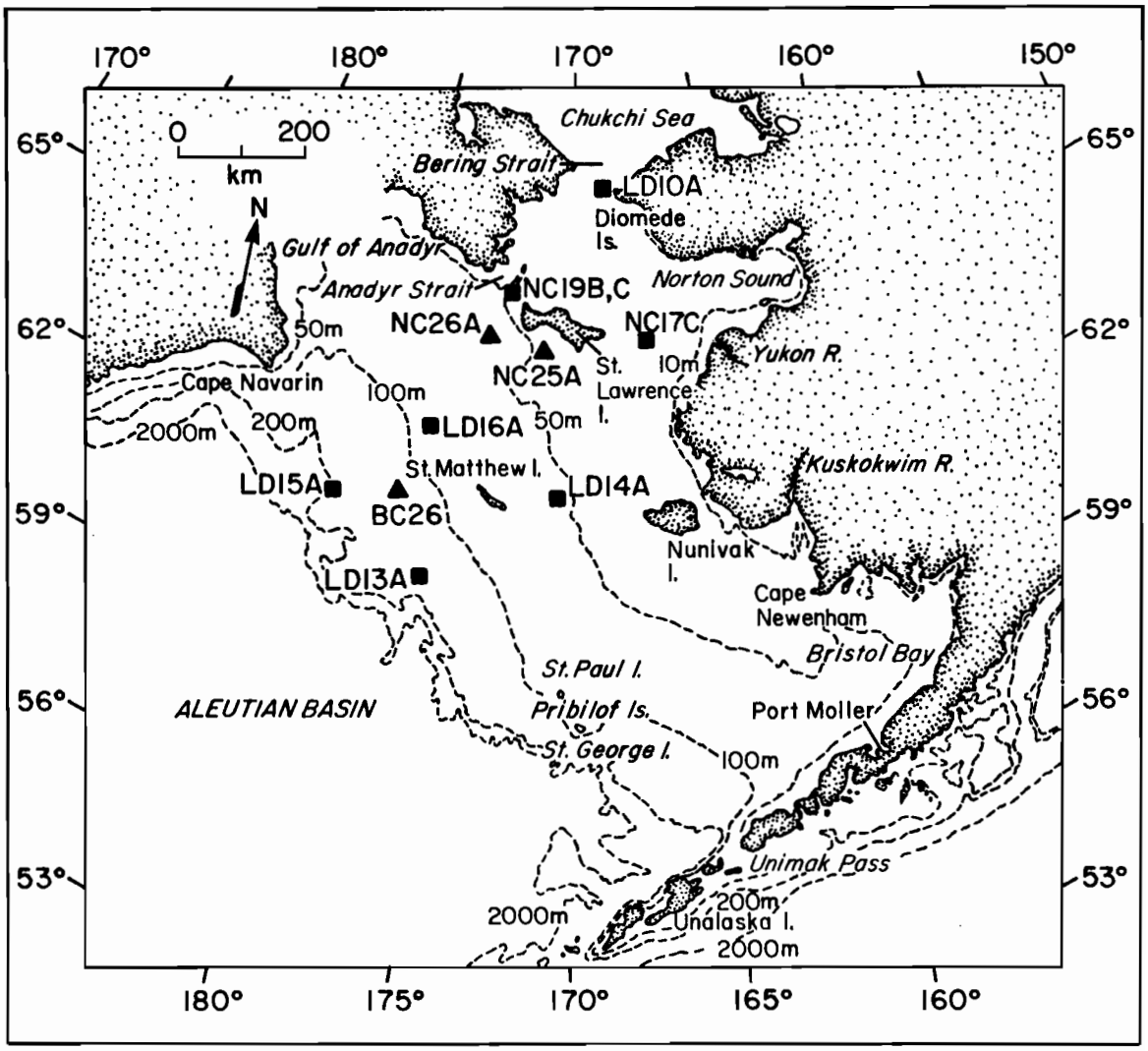

Figure 1. Locations of pressure and current stations on the Northeastern Bering Sea Shelf. The pressure stations are denoted by solid squares and the current stations by solid triangles.

currents that are the superpositions of tidal waves directly incident from the deep Aleutian Basin or through Bering Strait, propagating along coastlines, and reflecting from coasts and islands. One example of this is the semidiurnal M2 amphidrome predicted by the numerical model of Sündermann (1977) for the shelf off Cape Navarin.

Although the diurnal tides are strong on the Northeastern Bering Sea Shelf, they have received much less attention in the literature than the semidiurnal tides. On the outer shelf away from the coast, the diurnal tides should decay nearly exponentially in amplitude toward shore because the diurnal frequencies are less than the local Coriolis parameter (Fjeldstad, 1919; Munk, Snodgrass, and Wimbush 1970). We shall show that the diurnal tides on the outer shelf behave much like evanescent Sverdrup waves by comparing the observations with simple tidal theory.

2. OBSERVED TIDES

Pressure time series (Figs. 2 and 3) were obtained at seven stations (Fig. 1) using Aanderaa TG-3A pressure gages mounted firmly on bottom anchors. The time series were analyzed for pressure harmonic constants (Table 1 and Figs. 4-6), with sequences of 29-day harmonic analyses beginning every 15 days from the start of each time series. The pressure amplitudes in millibars (mb) can be multiplied by 0.993 to obtain amplitudes in centimeters (cm) for tidal height, based on representative values of the acceleration of gravity (982 cm s^{-2}) and the water density (1.026 g cm^{-3}) for the Northeastern Bering Sea Shelf. Two tide stations were actually deployed in Bering Strait. They give essentially identical tidal harmonic constants, and we present the results from the western station. The tides dominate the pressure time series (Figs. 2 and 3) on the outer

shelf. The tides diminish in amplitude and the non-tidal pressure fluctuations grow in intensity toward the north. In Bering Strait, the tides make a minor contribution compared with the non-tidal fluctuations.

The observations (Table 1 and Fig. 4) show that the diurnal tides decrease in amplitude from the shelfbreak toward the north and east. The K1 amplitude decreases from 38.7 mb (or 38.4 cm) at the shelfbreak station LD15A to 2.7 mb (or 2.7 cm) at the Bering Strait station LD10A. There is a similar decrease in the O1 amplitude from 26.0 mb (or 25.9 cm) at LD15A to 1.4 mb (or 1.4 cm) in Bering Strait. The observed diurnal phases are relatively constant (around 322°G to 346°G) over the open Northeastern Bering Sea Shelf, although Pearson *et al.* (1981) point out that diurnal amphidromic systems exist in the coastal regions near Nunivak Island and in Norton Sound where major changes occur locally in the diurnal phases. In Bering Strait, the observations have large fluctuations (Fig. 4) in the diurnal phases over the lengths of the time series.

The semidiurnal tides (Table 1 and Fig. 5) have greatly differing amplitudes at the seven stations (Fig. 1). The amplitudes on the outer shelf range from 21.6 mb (or 21.4 cm) at LD15A to 25.7 mb (or 25.5 cm) at NC17C. The exception is the M2 amplitude of 16.9 mb (or 16.8 cm) at LD16A which is under the influence of the M2 amphidromic system off Cape Navarin predicted by Sündermann (1977) and Liu and Leenderste (1982, 1984). The M2 amplitude of 7.7 mb (or 7.7 cm) at the Bering Strait station LD10A is a third of that on the outer shelf. The observed M2 phase is earliest at the shelfbreak (87°G at LD15A) and latest at NC17C (336°G).

The time series of tidal harmonic constants (Figs. 4 and 5) show little variations over seasonal time scales, except for the diurnal tide at the shelfbreak stations (LD13A and LD15A) and the semidiurnal M2 tide

Table 1a. Observed pressure harmonic constants[1] from recent tide stations (Fig. 1) on the Northeastern Bering Sea Shelf.

LD13A (depth = 130m)
59°04'N 175°08'W
4 Nov 1981 - 28 July 1982
(16 analyses)

	H (mb)		G°	
O1	23.3	0.3	318	1
P1	11.7	0.6	333	1
K1	35.2	1.4	334	1
N2	6.6	0.7	60	5
M2	22.8	0.2	106	1
S2	2.0	0.5	197	11

LD14A (depth = 57m)
60°34'N 170°36'W
31 Oct 1981 - 3 Aug 1982
(17 analyses)

	H (mb)		G°	
O1	9.1	0.7	304	4
P1	5.7	0.2	321	1
K1	17.3	0.7	322	1
N2	6.9	0.6	132	7
M2	22.1	0.8	180	1
S2	2.3	0.4	263	7

LD15A (depth = 196m)
60°44'N 178°52'W
3 Nov 1981 - 28 July 1982
(16 analyses)

	H (mb)		G°	
O1	26.0	0.3	318	1
P1	12.8	0.4	332	1
K1	38.7	1.2	333	1
N2	5.7	0.6	42	5
M2	21.6	0.2	87	1
S2	2.7	0.3	166	6

LD16A (depth = 80m)
61°53'N 175°00'W
3 Nov 1981 - 30 July 1982
(17 analyses)

	H (mb)		G°	
O1	12.2	0.8	325	3
P1	6.5	0.3	340	1
K1	19.6	0.9	341	1
N2	4.7	0.6	99	7
M2	16.9	0.4	145	1
S2	2.1	0.3	226	5

[1] Means and standard deviations based on overlapping 29-day harmonic analyses beginning every 15 days from the beginning of the time series. Multiply amplitudes in mb by 0.993 to obtain amplitudes in cm.

Table 1b. Observed pressure harmonic constants[1] from recent tide stations (Fig. 1) on the Northeastern Bering Sea Shelf.

NC17C (depth = 28m)
62°53'N 167°04'W
1 Nov 1981 - 2 Aug 1982
(17 analyses)

	H (mb)		G°	
O1	10.6	0.7	306	7
P1	6.2	0.4	343	5
K1	18.6	1.1	346	5
N2	7.8	0.8	281	12
M2	25.7	1.2	336	7
S2	3.0	0.7	53	13

NC19C (depth = 55m)
64°00'N 172°20'W
2 Nov 1981 - 11 June 1982
(12 analyses)

	H (mb)		G°	
O1	5.7	0.6	304	10
P1	3.3	0.2	326	3
K1	10.0	0.6	328	3
N2	6.2	0.5	118	7
M2	23.7	0.9	172	1
S2	2.7	0.4	252	14

LD10A (depth = 50m)
65°35'N 168°38'W
2 Nov 1981 - 1 Aug 1982
(17 analyses)

	H (mb)		G°	
O1	1.4	0.6	357	36
P1	0.9	0.2	359	28
K1	2.7	0.7	359	28
N2	2.4	0.5	128	13
M2	7.7	1.4	202	9
S2	1.4	0.7	312	38

[1] Means and standard deviations based on overlapping 29-day harmonic analyses beginning every 15 days from the beginning of the time series. Multiply amplitudes in mb by 0.993 to obtain amplitudes in cm.

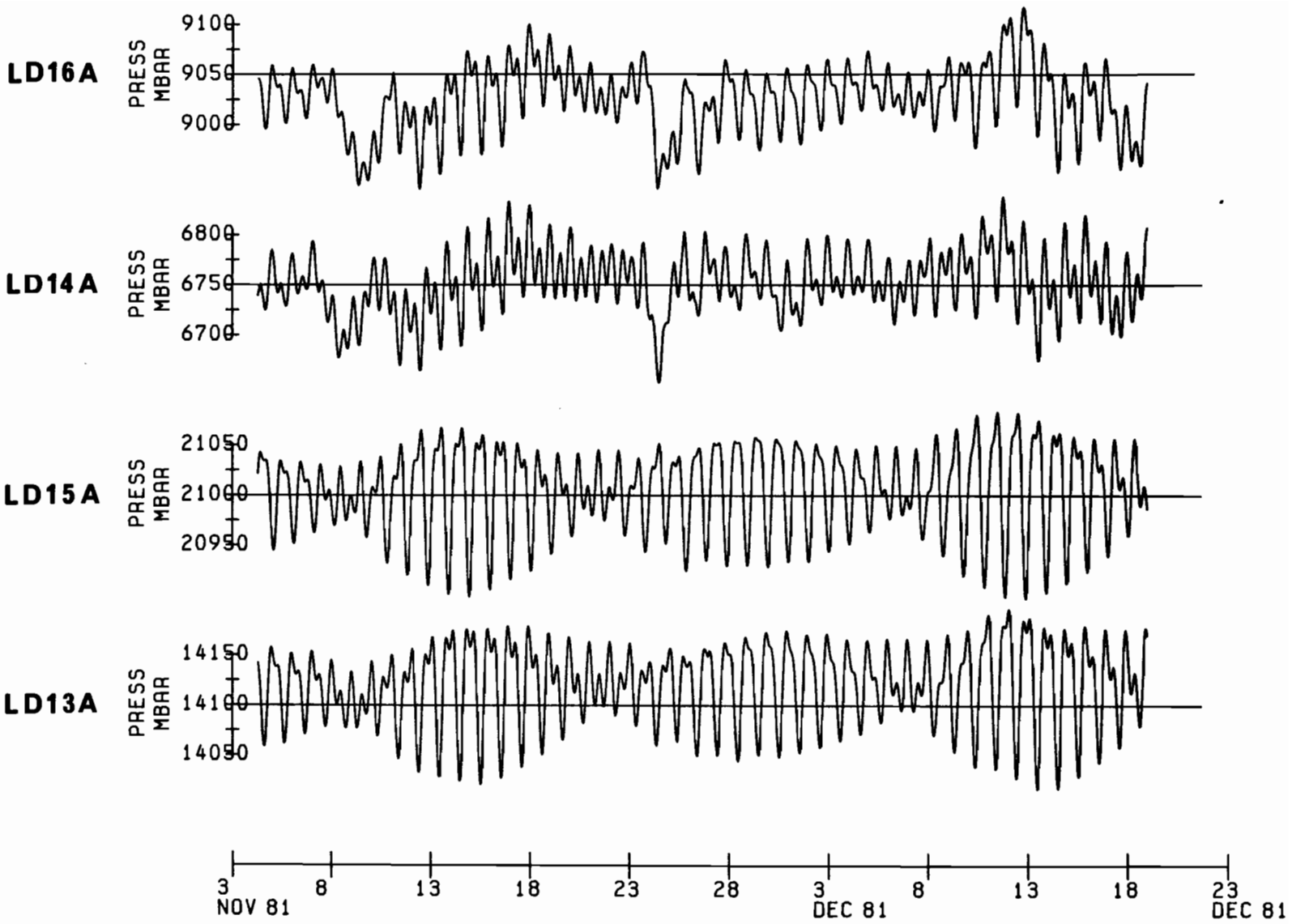

Figure 2. Examples of the pressure time series observed at stations (Fig. 1 and Table 1) on the Northeastern Bering Sea Shelf during November 1981 to August 1982.

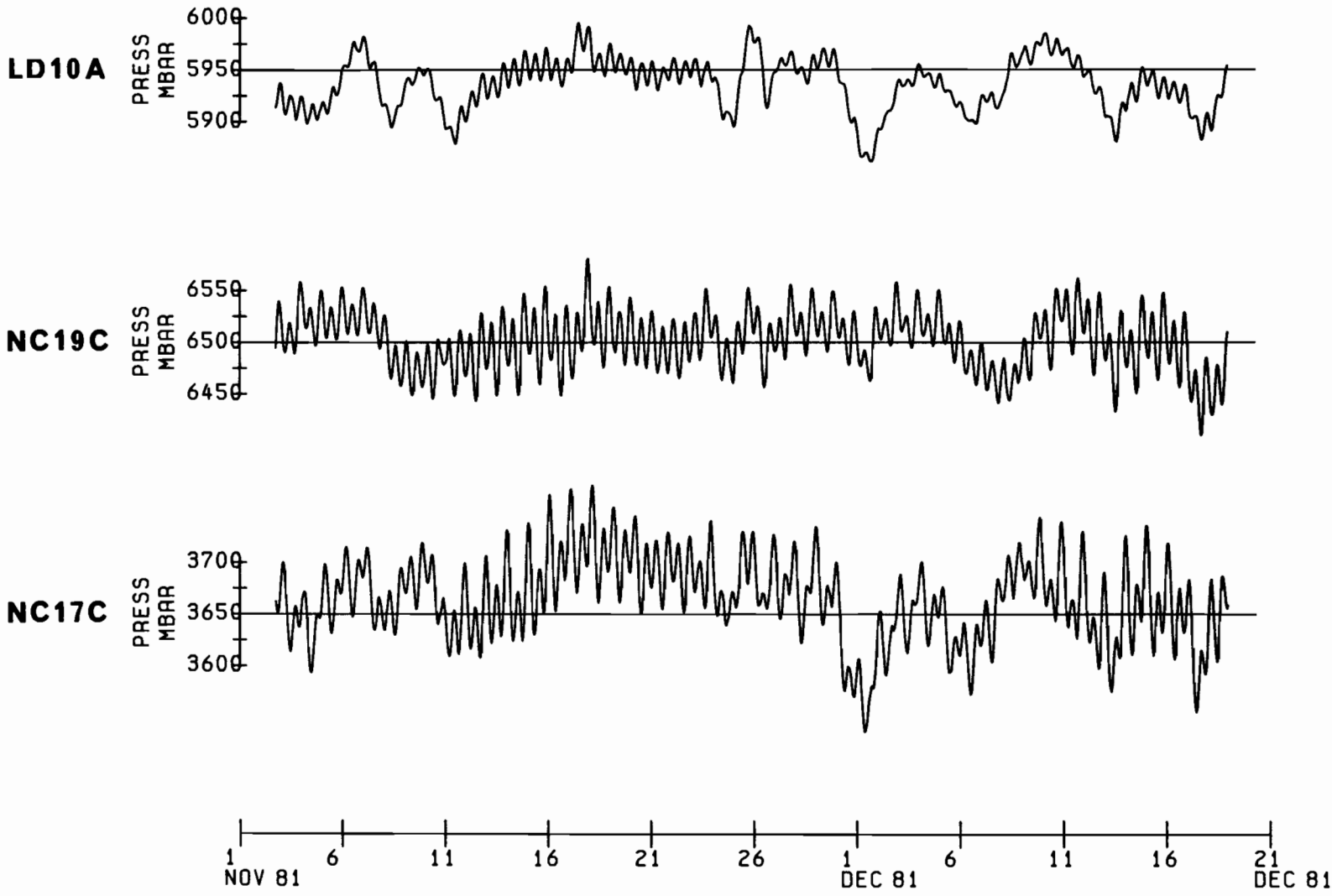

Figure 3. Examples of the pressure time series observed at stations (Fig. 1 and Table 1) on the Northeastern Bering Sea Shelf during November 1981 to August 1982 (cont.).

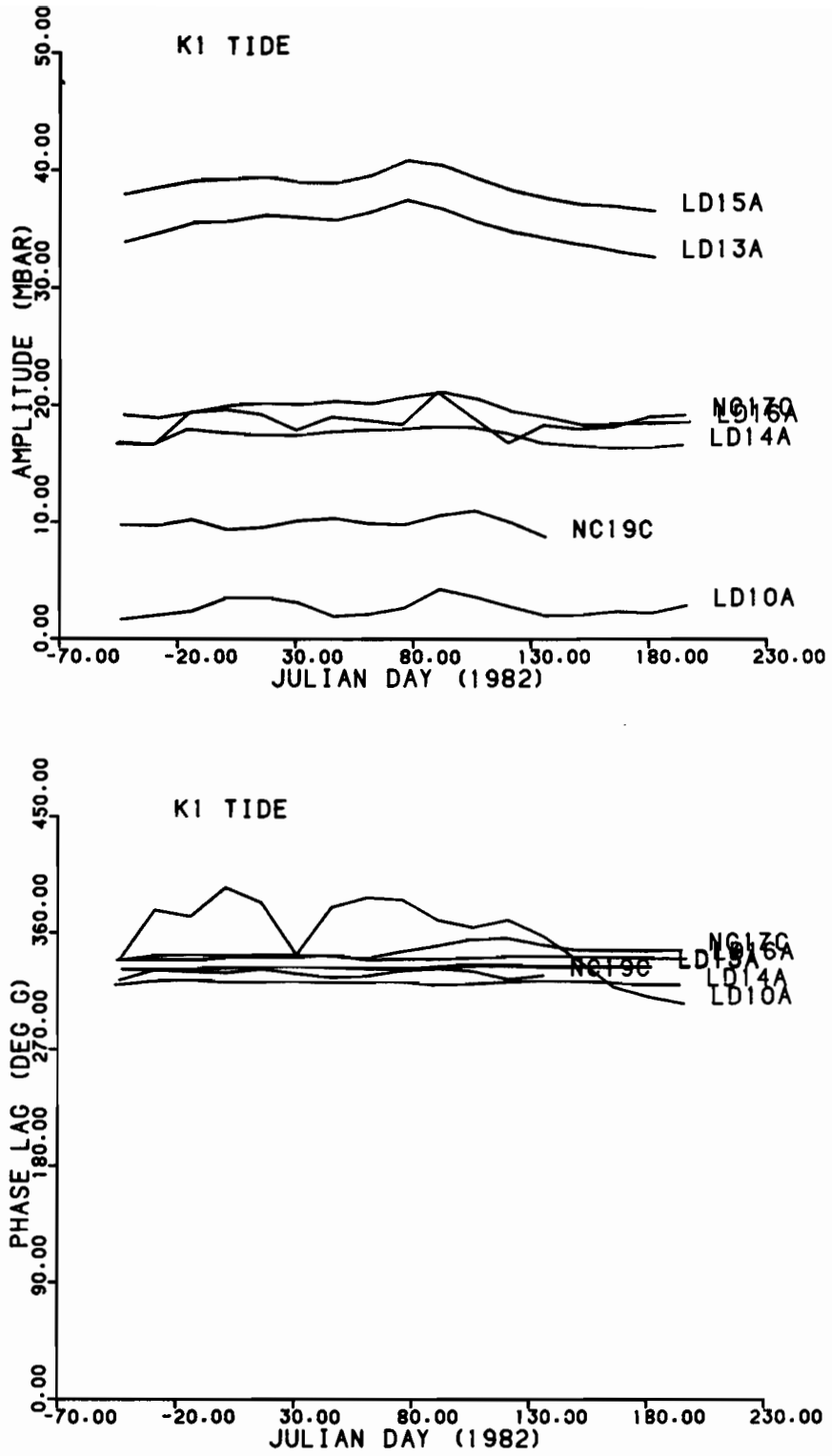

Figure 4. Time series of pressure harmonic constants for the K1 tide observed at stations (Fig. 1 and Table 1) on the Northeastern Bering Sea Shelf. Shown are the amplitudes (top) and Greenwich phase lags (bottom).

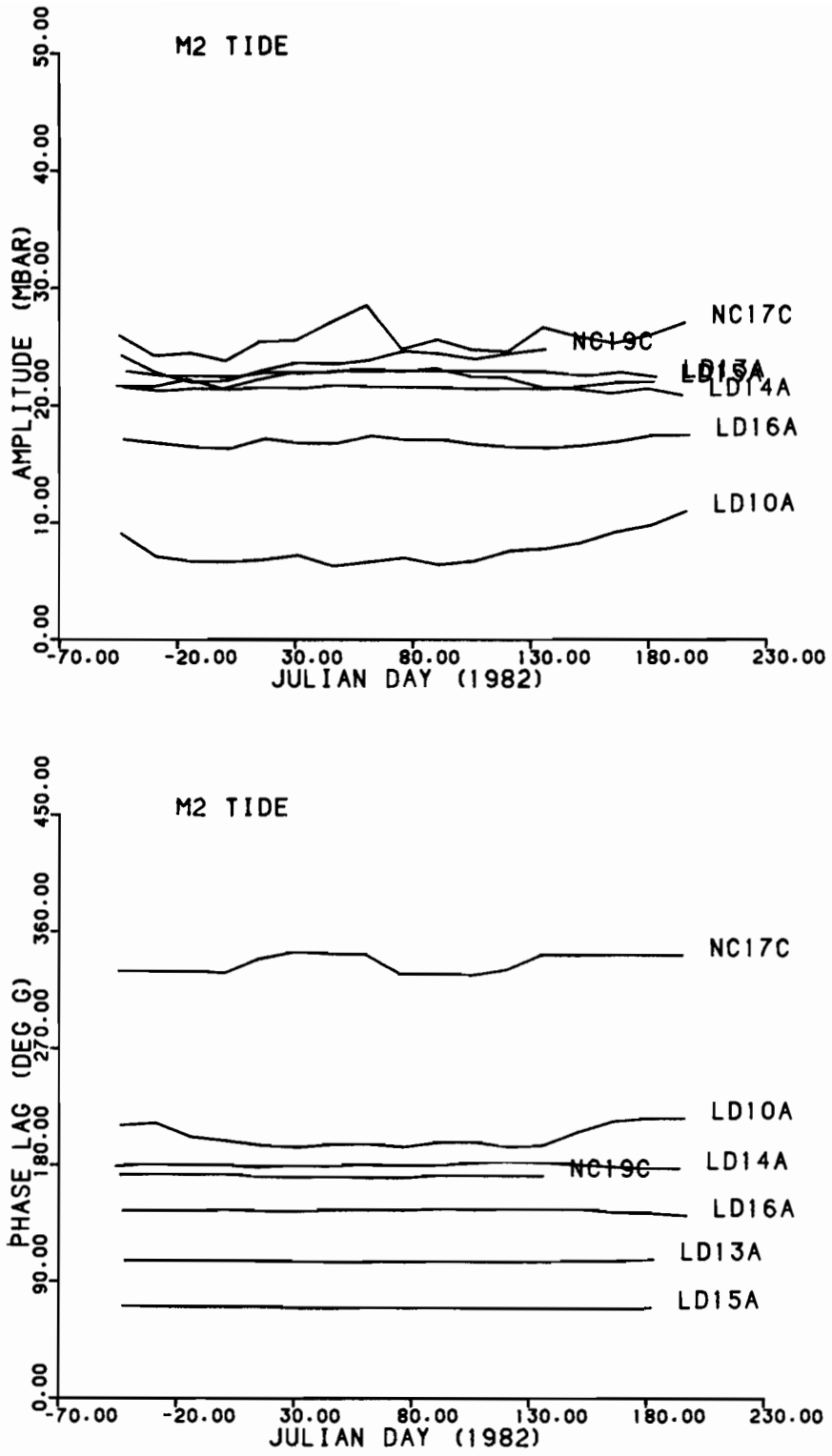

Figure 5. Time series of observed pressure harmonic constants for the M2 tide observed at stations (Fig. 1 and Table 1) on the Northeastern Bering Sea Shelf. Shown are the amplitudes (top) and Greenwich phase lags (bottom).

at the Bering Strait station (LD10A). Curiously, the K1 amplitudes at the shelfbreak stations show maximum values (~6% increase over the mean) during late winter (Day 80) while the M2 amplitude is a minimum (~18% decrease from the mean) in Bering Strait during the same period. We have no explanation for either variation at this time. It is tempting, however, to speculate that the lower M2 amplitudes in the Bering Strait during winter are due to attenuation of the M2 tidal waves by ice in the Bering Sea and the Arctic Ocean.

The Type of Tide (Table 2) indicates that the diurnal tides dominate the outer shelf stations. The tidal regime changes northward and eastward from LD13A and LD15A until it is semidiurnal in Bering Strait. The Sequence of Tides (Table 2) at the shelfbreak (174° at LD13A and 156° at LD15A) gives a sequence of two nearly equal high waters (Fig. 2) separated by greatly differing low waters for those times when the moon is at high declination (tropic tides). There is considerable variation in the Sequence of Tides between the other stations.

3. OBSERVED TIDAL CURRENTS

Current observations are rare in the western region of the Northeastern Bering Sea Shelf. We shall focus on four current stations (Fig. 1) selected from those presented by Salo, Schumacher, and Coachman (1983). These authors discuss the general aspects of the tidal and other currents. We extend the discussion by presenting current harmonic constants. The current time series (Fig. 6) were obtained during November 1980 to June 1981 with Aanderaa RCM-4 current meters attached to taut-wire moorings below subsurface floats. One of the moorings BC26 was deployed by R. Muench (Science Applications, Inc.) while the others were deployed by R. Tripp

Table 2. Tidal characteristics at pressure stations (Fig. 1) recently occupied on the Northeastern Bering Sea Shelf.

Station	Type[1] of Tide	Sequence[2] of Tide°
LD13A	1.99	174
LD14A	0.91	274
LD15A	2.37	156
LD16A	1.47	199
NC17C	0.87	44
NC19C	0.53	260
LD10A	0.41	206

[1] (K1+O1)/(M2+N2) where N2 has been substituted for S2 in the standard formula because S2 is anomalously small in the Bering Sea (Pearson, Mofjeld, and Tripp, 1981).

[2] M2° - K1° - O1°

(University of Washington). The current time series were analyzed for tidal current harmonic constants (Table 3 and Figs. 7, 8 and 9) using overlapping 29-day harmonic analyses beginning every 15 days from the start of each time series.

Located 170 km east of St. Matthew Island, the current station BC26 has broad tidal current ellipses (Table 3 and Fig. 7) with comparable diurnal and semidiurnal amplitudes (K1+O1 = 13.6 cm/s and M2+N2 = 13.8 cm/s). The diurnal and semidiurnal orientations are at right angles with the major axis of the K1 ellipse oriented 85°±9° counterclockwise from that of the M2 ellipse at BC26. The major axis of the M2 ellipse is perpendicular to the general trends of the shelfbreak and the isobaths in this region of the shelf. The K1 current along its major axis is close to 180° out of phase with the K1 tides at the surrounding pressure stations (Tables 1a and 3), while the M2 current is slightly later in phase (154° at BC26 versus 145° at the pressure station LD16A) than the M2 tide observed nearby. All the major constituents have a clockwise sense of rotation. As we shall see in the next section, the tides and tidal currents on the outer shelf have much in common with Sverdrup waves incident from the Aleutian Basin.

Kitani and Kawasaki (1979) report tidal current observations from the outer shelf region of the Northeastern Bering Sea Shelf. The tidal ellipses that they present are also broad, and the diurnal and semidiurnal ellipses are at right angles to each other. They found much larger current amplitudes near the surface than at deeper depths. This may be due to the use of slack-wire moorings with surface floats, which allow rotor-pumping by surface waves to enhance the apparent speeds of the near-surface currents. Theoretical calculations of current profiles by the present author show

Table 3. Current harmonic constants[1] from selected current stations on the Northeastern Bering Sea Shelf.

BC26 (current meter at 50 m depth; total depth = 119 m)
60°34'N 176°02'W
13 Nov 1980 - 4 June 1981 (12 analyses)

	Amplitudes (cm/s) Major		Minor		Phase Lag (degrees G)		Orientation (degrees True)		Sense of Rotation
O1	5.4	0.4	3.5	0.5	146	5	318	6	C
P1	2.7	0.1	2.0	0.1	162	7	319	7	C
K1	8.2	0.3	6.1	0.3	163	7	319	7	C
N2	3.4	0.4	2.5	0.4	102	15	47	13	C
MC	10.4	0.3	7.9	0.4	154	8	44	5	C
S2	1.3	0.3	1.0	0.1	283	55	123	47	C

NC19B (current meter at 45 m depth; total depth = 55 m)
63°58'N 172°01'W
12 Nov 1980 - 29 June 1981 (14 analyses)

	Amplitudes (cm/s) Major		Minor		Phase Lag (degrees G)		Orientation (degrees True)		Sense of Rotation
O1	1.7	0.4	0.0	0.2	326	10	47	6	(C)
P1	1.0	0.1	0.0	0.1	353	9	46	4	(C)
K1	3.0	0.4	0.0	0.2	355	9	46	4	(C)
N2	1.3	0.3	0.1	0.4	136	26	69	20	(CC)
M2	5.3	0.4	0.6	0.5	190	12	62	8	(CC)
S2	1.1	0.4	0.1	0.3	110	44	237	47	(CC)

NC25A (current meter at 36 m depth; total depth = 46 m)
63°00'N 170°58'W
12 Nov 1980 - 29 June 1981 (14 analyses)

	Amplitudes (cm/s) Major		Minor		Phase Lag (degrees G)		Orientation (degrees True)		Sense of Rotation
O1	1.2	0.3	0.3	0.3	188	18	293	7	(C)
P1	0.6	0.1	0.1	0.1	212	10	292	9	(C)
K1	1.8	0.4	0.4	0.2	214	10	292	9	C
N2	1.3	0.3	0.1	0.2	4	11	306	17	CC
M2	4.8	0.7	0.2	0.5	62	6	299	5	(CC)
S2	0.8	0.3	0.1	0.2	122	61	335	49	(C)

NC26A (current meter at 57 m depth; total depth = 67 m)
63°11'N 173°08'W
12 Nov 1980 - 29 June 1981 (14 analyses)

	Amplitudes (cm/s) Major		Minor		Phase Lag (degrees G)		Orientation (degrees True)		Sense of Rotation
O1	1.0	0.3	0.5	0.2	202	21	308	15	C
P1	0.4	0.1	0.2	0.1	218	17	304	15	C
K1	1.3	0.2	0.7	0.2	219	17	304	14	C
N2	1.0	0.3	0.5	0.3	36	21	348	19	C
M2	3.1	0.7	1.1	0.4	104	5	349	4	C
S2	0.6	0.3	0.2	0.2	186	40	354	46	(C)

[1] Means and standard deviations based on overlapping 29-day harmonic analyses beginning every 15 days from the start of each time series.

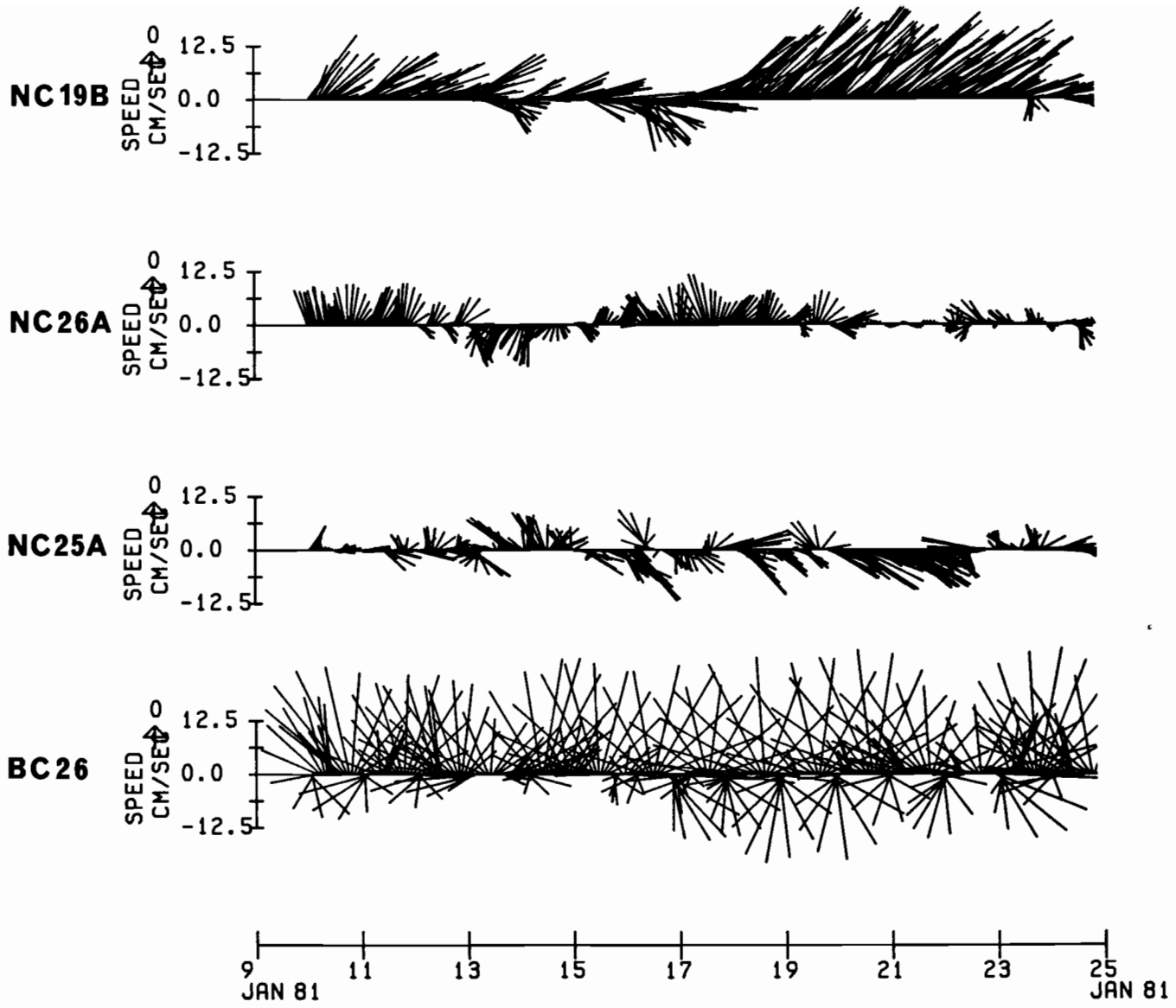

Figure 6. Examples of current time series observed at stations (Fig. 1 and Table 3) on the Northeastern Bering Sea Shelf during November 1980 to June 1981.

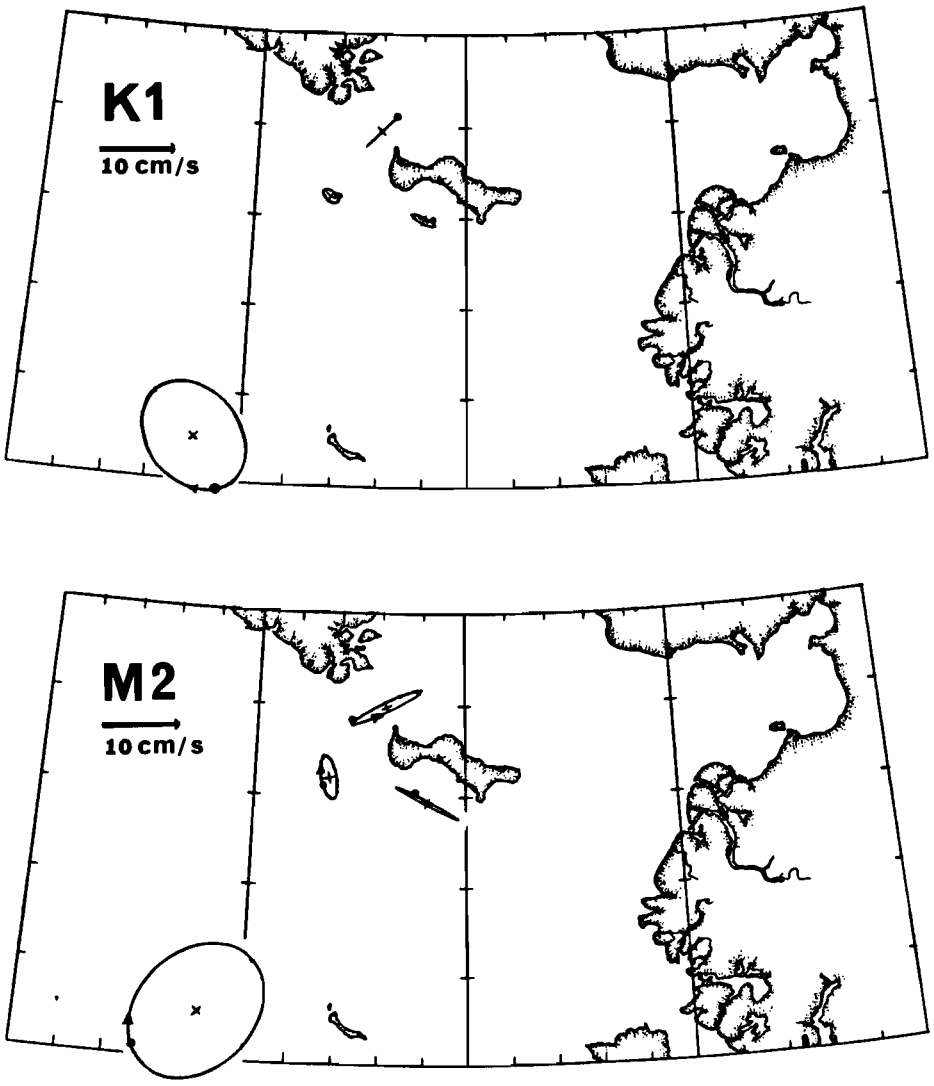

Figure 7. Tidal current ellipses for K1 (top) and M2 (bottom) observed at stations (Fig. 1 and Table 3) on the Northeastern Bering Sea Shelf.

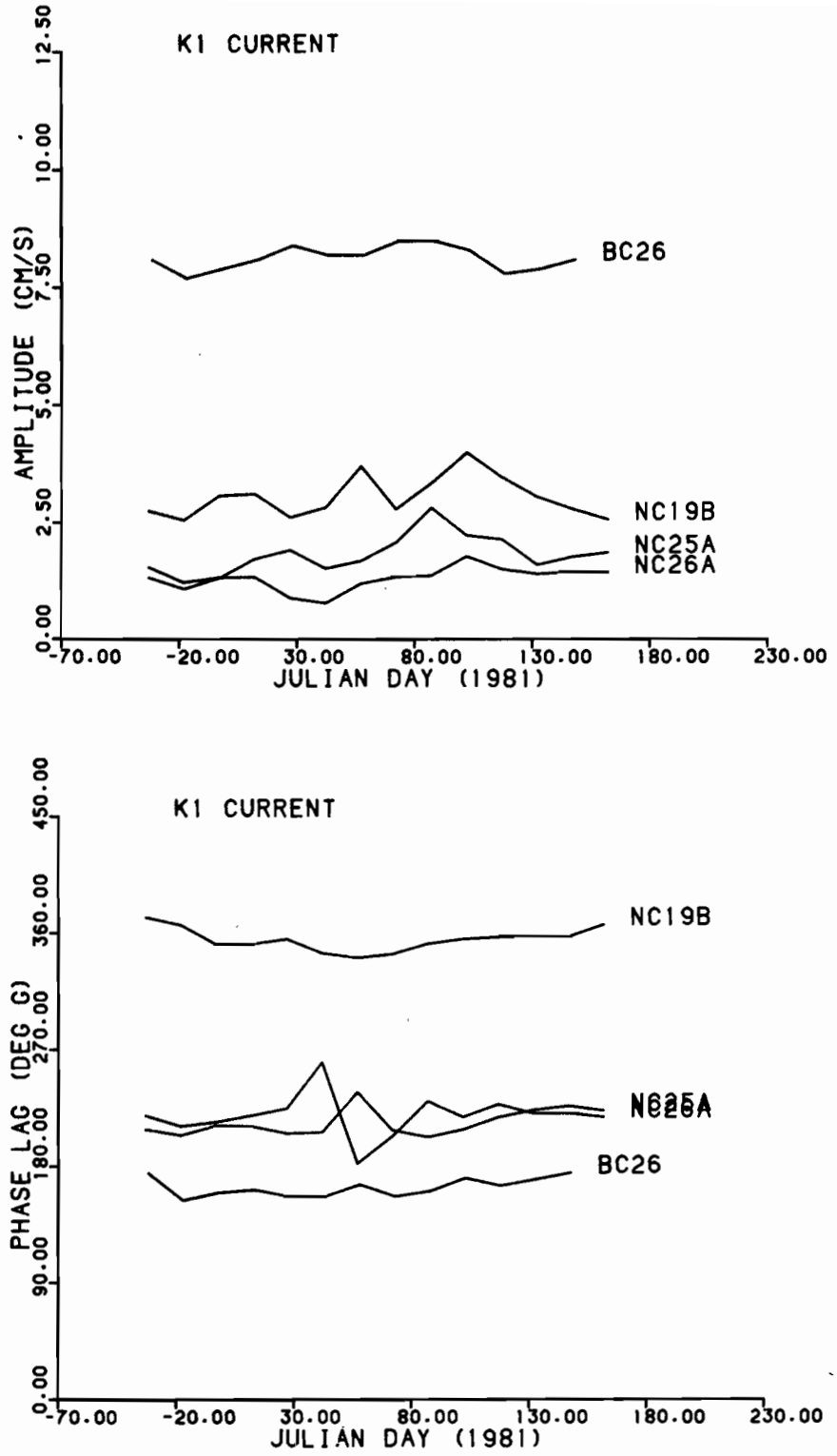

Figure 8. Time series of observed current harmonic constants for the K1 tidal currents at stations (Fig. 1 and Table 3) on the Northeastern Bering Sea Shelf. Shown are the amplitudes (top) and Greenwich phase lags (bottom) along the major axes.

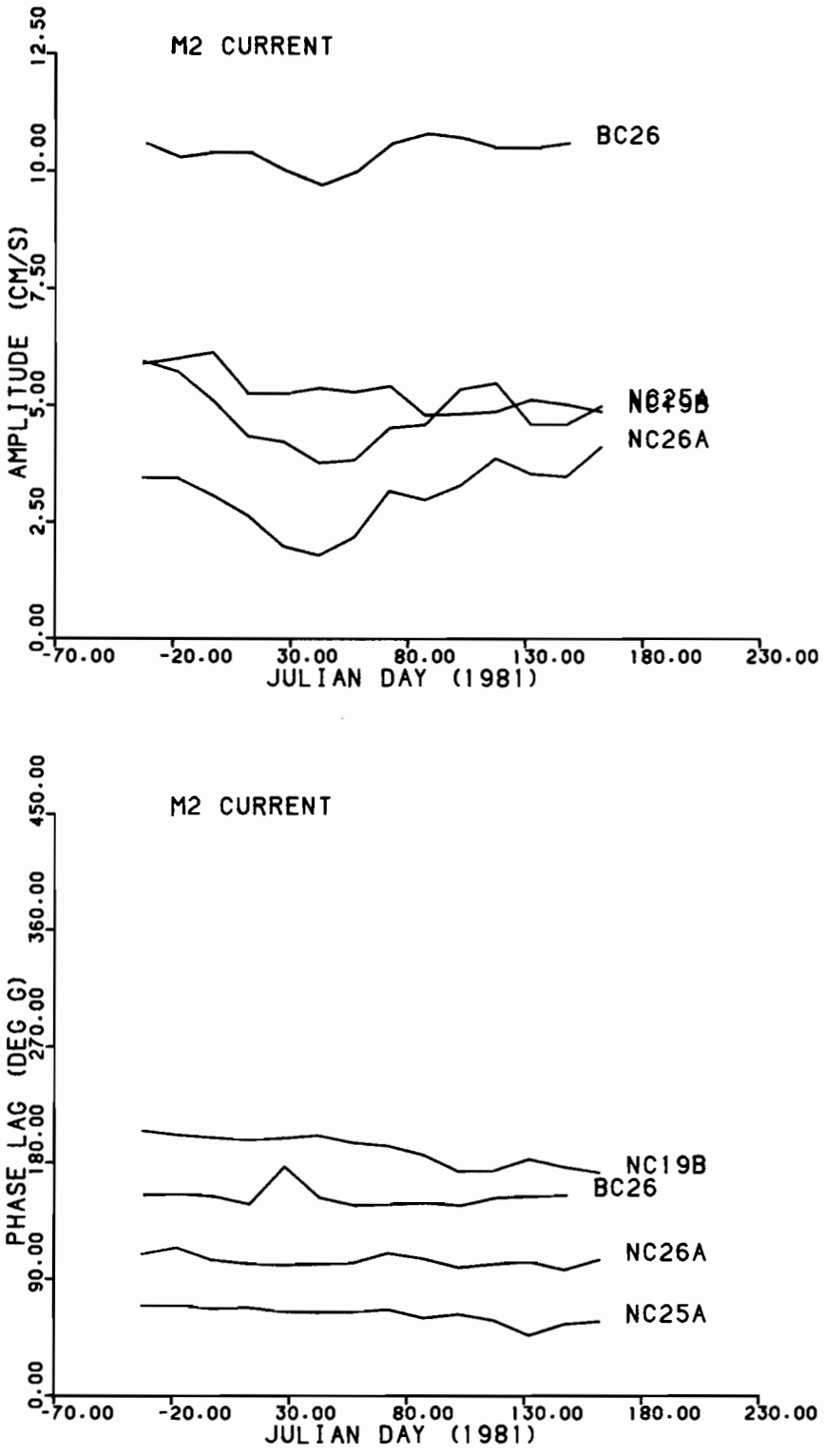

Figure 9. Time series of observed current harmonic constants for the M2 tidal currents at stations (Fig. 1 and Table 3) on the Northeastern Bering Sea Shelf. Shown are the amplitudes (top) and Greenwich phase lags (bottom) along the major axes.

that the bottom shear layer does not extend high into the water column for tidal ellipses typical of the outer shelf; this is supported by bottom layer observations made between Nunivak and the Pribilof Islands. It therefore seems unlikely that the apparent current shear profiles observed by Kitani and Kawasaki (1979) are real.

The other current stations (Fig. 1 and Table 3) are located in the vicinity of St. Lawrence Island. The current amplitudes are roughly half (around 5 cm/s for M2) of those at the outer shelf station BC26, and the semidiurnal currents dominate the tidal regime. The tidal currents at the station NC19B in Anadyr Strait are oriented along the axis of the strait and have phase lags somewhat later (27° for K1 and 18° for M2) than the tides observed at NC19C (Table 1b) in Anadyr Strait. The orientations of the tidal currents at NC25A and NC26A are roughly parallel to the adjacent coast of St. Lawrence Island. Their phases are significantly earlier than those at NC19B in Anadyr Strait although they are relatively close by. The tidal ellipses at NC19B and NC25A are essentially rectilinear, while those at NC26A are broader and have a clockwise sense of rotation.

Time series of current harmonic constants (Figs. 8 and 9) reveal some variation over seasonal time scales. There is a tendency of the small K1 current amplitudes (Fig. 8) near St. Lawrence Island to be larger than the mean (33% for NC19B, 57% for NC25A, and 37% for NC26A) in late winter and early spring (centered approximately on Julian Day 90) than at the beginnings and ends of the records and for the K1 phase in Anadyr Strait (NC19B) to be slightly earlier during the same period. The K1 tide (Fig. 4) observed a year later also shows an increase in amplitude during the same season. The phase lag (Fig. 4) of the K1 tide is unchanged over the time series except for a substantial increase in K1 tidal phase lag in Bering Strait.

The largest variations appear in the M2 current amplitudes (Fig. 9) at stations NC25A and NC26A near St. Lawrence Island. There is a 51% decrease in the M2 amplitude (3.5 cm/s) at NC25A from the beginning of the record (Julian Day 317 1980) to a minimum value (1.8 cm/s) occurring around Julian Day 40. The decrease is 42% at NC26A. A smaller decrease (7%) in M2 current amplitude (Fig. 9) can be seen at the outer shelf station BC26. The M2 phases (Fig. 9) tend to become progressively earlier through the records.

Pearson, Mofjeld, and Tripp (1981) report significant variations in the M2 currents at the upper meter (24 m depth) of two current meters deployed during September 1977 to September 1978 at a station NC24 (61°48'N, 170°26'W) located about half way between St. Matthew Island and the eastern end of St. Lawrence Island. The lower current meter (40 m depth) had a relatively constant M2 current amplitude with an initial increase in the M2 phase lag. During the period of heavy ice cover (February to April 1978), the M2 current amplitude at the upper meter decreased from an initial value of 22 cm/s until is was essentially equal to that (14 cm/s) at the lower meter. One explanation for the variation in M2 amplitude is the suppression by ice of wave-induced rotor pumping which made the amplitude at the upper meter artifically high. As with the current observations of Kitani and Kawasaki (1979), theoretical calculations of current profiles do not show large variations in tidal current with height well above the bottom when ice is not present.

At present, the effects of ice on the tides and tidal currents on the Eastern Bering Sea Shelf are unknown; but the observations presented here suggest that these effects are not major on the outer shelf. The M2 tide in Bering Strait varies considerably with season which suggests the

influence of ice in the Arctic Ocean and the Bering Sea. The M2 tidal currents near St. Lawrence Island are also found to vary. Numerical simulations and detailed observations of current profiles are needed to define the regional extent and dominant mechanisms of ice influence on the tides and tidal currents of the Northeastern Bering Sea Shelf.

4. DISCUSSION

4.1 Sverdrup Wave Theory

It is interesting to compare the tides and tidal currents observed on the outer shelf with simple tidal theory. Several features of the tides at LD13A, LD15A, and LD16A (Table 1) and the tidal currents at BC26 (Table 3) suggest that the tidal motions in this region closely resemble Sverdrup waves incident from the Aleutian Basin. These features include: the marked decrease in diurnal amplitudes with distance shoreward of the shelfbreak, the relatively constant phase lags of the diurnal tides, the broad, clockwise-rotating tidal currents, and the orientations of these ellipses relative to the isobaths. We shall test this idea by comparing the observations with predictions based on Sverdrup wave theory.

Each tidal constituent has a single wave of the form

$$(u,v,\eta) = (u_o,v_o,\eta_o)\ \exp[i(k_x X - \omega t)] \qquad (1)$$

The Sverdrup waves are assumed to satisfy the linear, inviscid, barotropic equations for long, free waves on a shelf of constant depth

$$-i\omega u - fv = -igk_x\eta \qquad (2)$$

$$-i\omega v + fu = 0 \qquad (3)$$

$$-i\omega\eta + iHk_x u = 0 \qquad (4)$$

with cross-shelf u and along-shelf v velocity components, surface elevation η, angular frequency ω, Coriolis parameter f, acceleration of gravity g, cross-shelf wavenumber component k_x, and depth H. The along-shelf wavenumber component k_y is set equal to zero under the assumptions that the along-shelf spatial scales are set by the long waves in the deep Aleutian Basin and that these scales are much longer than those of the cross-shelf variations.

Equations (2)-(4) lead to the dispersion relations

$$k_x = i\beta,\ \beta = [(f^2 - \omega^2)/gh]^{\frac{1}{2}} \quad \text{for } \omega < f \qquad (5)$$

$$k_x = [(\omega^2 - f^2)/gh]^{\frac{1}{2}} \quad \text{for } \omega > f \qquad (6)$$

The changes in tidal amplitudes with cross-shelf distance X are

$$\eta = \eta(\text{ref})e^{-\beta X} \quad \text{for } \omega < f \qquad (7)$$

$$\eta = \eta(\text{ref}) \quad \text{for } \omega > f \qquad (8)$$

while the corresponding tidal phase shifts with cross-shelf distance are

$$\phi_x = 0° \quad \text{for } \omega < f \qquad (9)$$

$$\phi_x = k_x X \quad \text{for } \omega > f \qquad (10)$$

The tidal currents can also be used to obtain estimates of the tides; from Equations (3) and (4),

$$\eta = -H\beta v/f \quad \text{for } \omega < f \qquad (11)$$

$$\eta = Hk_x u/\omega \quad \text{for } \omega > f \qquad (12)$$

The relative phases of the current components along the major axes with respect to the tides are

$$\Delta\phi = 180° \quad \text{for } \omega < f \qquad (13)$$

$$\Delta\phi = 0° \quad \text{for } \omega > f \qquad (14)$$

The ratios of current amplitudes (minor component/major component) are

$$|u/v| = \omega/f \qquad \text{for } \omega < f \qquad (15)$$

$$|v/u| = f/\omega \qquad \text{for } \omega > f \qquad (16)$$

Finally, the orientations of the major current axes relative to the isobaths (assuming that the isobaths are parallel to a straight shelfbreak) are

$$\phi_b = 0° \qquad \text{for } \omega < f \qquad (17)$$

$$\phi_b = 90° \qquad \text{for } \omega > f \qquad (18)$$

The comparison (Table 4) of the observations at LD16A and BC26 with theoretical predictions show that the tides and tidal currents on the outer Bering Sea Shelf have much in common with Sverdrup waves. The observed diurnal K1 tides decrease in amplitude at the appropriate rate moving inshore from the shelfbreak, and the K1 phase lag is relatively constant over the region. The Sverdrup wave predicts consistent amplitudes and phases for the K1 tide at BC26 inferred from amplitude decay and the K1 current. It also predicts the orientation of the K1 ellipse and the sense of rotation. The current ratio (Table 4) determining the breadth of the K1 ellipse is not predicted well - the observed K1 ellipse is significantly broader than that for a Sverdrup wave. The distance of 322 km from Cape Navarin (62°20'N, 179°10'E) to BC26 is comparable with the Rossby radius $(gH)^{\frac{1}{2}}/f$ = 267 km, assuming a mean depth of 119 m (same as that at BC26). Since the Rossby radius is the e-folding decay scale for Kelvin waves extending outward from Cape Navarin, the diurnal tidal motions at BC26 are effected by these Kelvin waves. The observed diurnal K1 ellipse at BC26 may be broader than predicted from

Table 4. Predictions[1] of tides at LD16A and NC26 and properties of the tidal current at NC26 based on inviscid Sverdrup wave theory.

	Observed	Sverdrup Wave	Equations
Diurnal Constituent K1			
LD16A			
Tidal Amplitude	19.5 0.9 cm	21.0 0.7 cm	(5) and (7)
Tidal Phase Lag	341° 1°G	333° 1°G	(9)
NC26			
Tidal Amplitude	--	24.6 0.8 cm	(7)
Tidal Amplitude	--	23.3 0.9 cm	(11)
Phase Difference (v rel. to η)	186° 7°	180°	(13)
Current Ratio	0.74 0.06	0.58	(15)
Orientation	319° 7°T	335° T	(17)
Rotation	Clockwise	Clockwise	
Semidiurnal Constituent M2			
LD16A			
Tidal Amplitude	16.8 0.4 cm	21.4 0.2 cm	(8)
Tidal Phase Lag	145° 1°G	107° 1°G	(10)[2]
NC26			
Tidal Amplitude	--	19.1 0.4 cm	(8)[2]
Tidal Amplitude	--	15.7 0.5 cm	(12)
Phase Difference (u rel. to n)	38° 8°	0°	(14)
Current Ratio	0.76 0.06	0.90	(16)
Orientation	44° 5°T	65° T	(18)
Rotation	Clockwise	Clockwise	

[1] Amplitudes and phases from Tables (1) and (3); $f = 1.266\ (10)^{-4}\ s^{-1}$, $g = 982\ cm\ s^{-2}$, $H = 119$ m, $X = 147$ km between LD15A and BC26, $X = 199$ km between LD15A and LD16A, $\omega = 0.729\ (10)^{-4}\ s^{-1}$ for K1, and $\omega = 1.405\ (10)^{-4}\ s^{-1}$ for M2.

[2] Prediction based on mean of values at LD15A and LD16A.

Sverdrup wave theory because of a K1 Kelvin wave reaching out to the station from the Siberian Coast.

The predicted M2 tides and tidal currents (Table 4) agree less well with the observations at LD16A and BC26. One interpretation of this result is that the M2 tidal motions are the superposition of several waves. Sündermann (1977) and Liu and Leenderste (1982, 1984) find an M2 amphidromic system off Cape Navarin in numerical tidal models of the Bering Sea Shelf. The semidiurnal tide and tidal currents at LD16A and BC26 are under the influence of this system, which may be thought of as a superposition of incident waves from the Aleutian Basin together with Kelvin waves propagating toward the shelfbreak along the Siberian Coast. Battisti and Clarke (1982) find that along-shelf variations and friction can cause the M2 ellipses to be narrower than the ratio ω/f.

4.2 Numerical Models

There are two numerical models of the tides on the Eastern Bering Sea Shelf that can be compared (Table 5) with the tidal observations on the outer shelf. One of these is the vertically-integrated model of M2 by Sündermann (1977), and the other is the three-dimensional model by Liu and Leenderste (1982, 1984) which provides preliminary estimates of composite diurnal and semidiurnal tides. The tidal observations reported in this memorandum were taken to provide boundary conditions and interior test data for the three-dimensional model. The comparison that we shall present uses values from a preliminary version of the model which has not been tuned to these observations. A refined version of the model is presently under development (Liu, private communication, 1984). In Table 5, the

Table 5. Comparison of observed tides with predictions of numerical models for the tides on the Northeastern Bering Sea Shelf.

M2 Tide from Sündermann (1977)

Station	Observed H (cm)	Observed G°	Model[1] H (cm)	Model[1] G°
LD13A	22.7	106	~36 (~23)	~115
LD14A	22.0	180	~39 (~25)	150
LD15A	21.5	87	~31 (~21)	~115
LD16A	16.8	145	~28 (~20)	~140
NC17C	25.5	336	~15 (~10)	330
NC19C	23.6	172	~23 (~20)	~240
LD10A	7.7	202	~10 (~ 6)	~230

Composite Diurnal Tide (Preliminary) from Liu and Leenderste (1982, 1984)

Station	Observed[2] H (cm)	Observed[2] G°	Model H (cm)	Model G°
LD13A	28.4	334	28	~330
LD14A	14.0	322	~17	~320
LD15A	31.4	334	28	~330
LD16A	15.8	341	16	330
NC17C	15.1	346	~12	~ 5
NC19C	8.0	329	10	~339
LD10A	2.2	359	~ 2	~330

Composite Semidiurnal Tide (Preliminary) from Liu and Leenderste (1982, 1984)

Station	Observed[3] H (cm)	Observed[3] G°	Model H (cm)	Model G°
LD13A	28.8	106	--	~103
LD14A	27.9	180	~25	~175
LD15A	27.3	87	~23	~ 90
LD16A	21.4	145	~18	~135
NC17C	32.5	336	~30	~310
NC19C	30.0	172	--	~180
LD10A	9.7	202	~ 8	~130

[1] Amplitudes in parentheses have been multiplied by a factor of 0.65 to adjust the model so that its amplitude matches the observed M2 amplitude at the Pribilof Islands.

[2] Amplitudes based on Q1, O1, P1, and K1 for 2-3 August 1976; phases same as those for K1.

[3] Amplitudes based on N2, M2, S2, and K2 for 2-3 August 1976; phases same as those for M2.

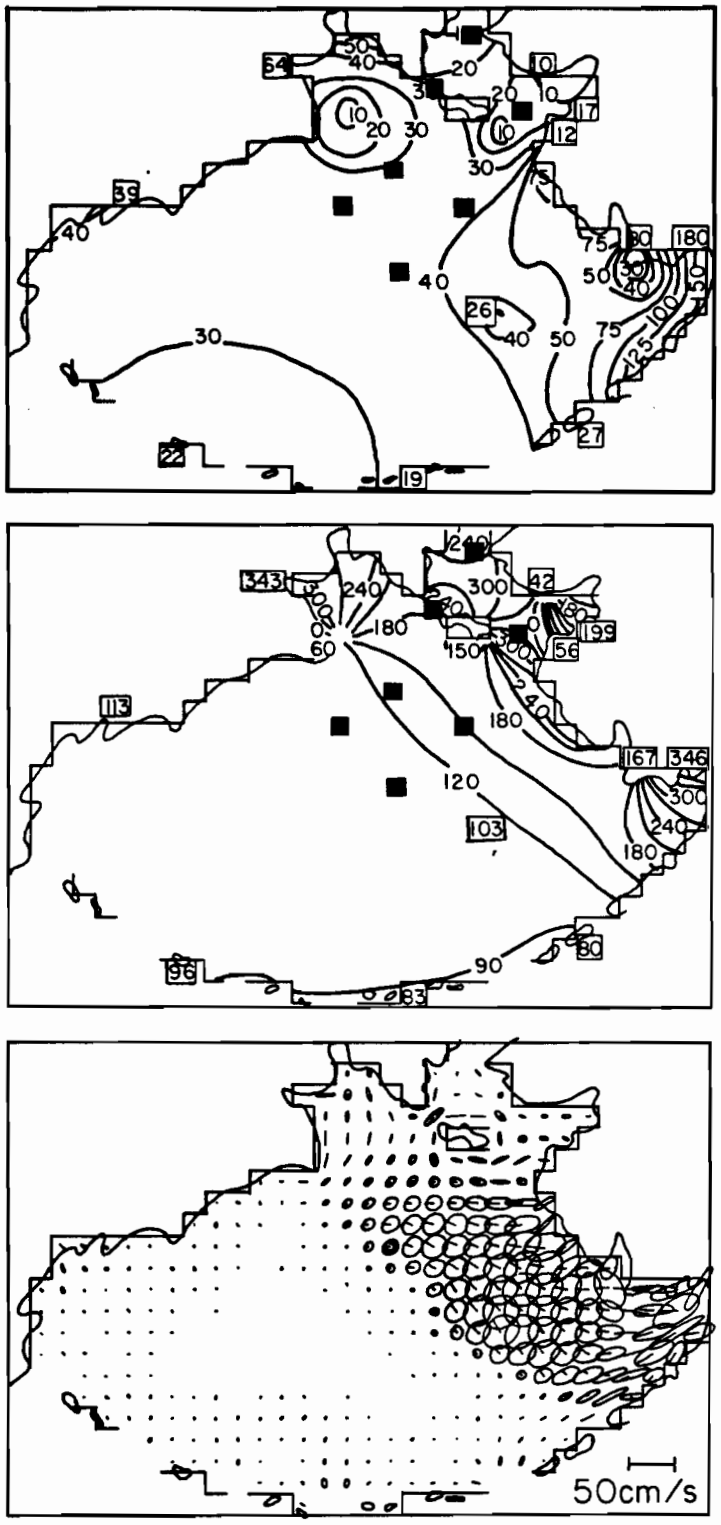

Figure 10. M2 tide and tidal currents in the Bering Sea from a vertically-integrated model by Sünderman (1977). Shown in the top plate are co-amplitude lines (cm), in the middle plate are cophase lines (degrees G), and in the bottom plate are current ellipses. Also shown are observed values (in open squares) used to tune the model and locations (solid squares and partially filled ellipses) for which comparisons (Tables 5 and 6) are made between the model and observations. (Modified slightly from J. Sündermann, 1977, *Deutsche Hydrographische Zeitschrift*, 91-101, Figs. 3, 4, 5).

missing amplitudes for the composite semidiurnal tides and the approximate symbols indicate some difficulty in estimating theoretical amplitudes and phases at the tide stations from the theoretical cotidal charts.

The comparison (Table 5) of the observations at the seven tide stations (Fig. 10) with the predicted M2 tide by Sündermann (1977) shows good qualitative agreement, although the model gives larger M2 amplitudes and later phase lags than are seen in the observations. The tide amplitudes predicted by Sündermann (1977) can be brought into relatively close agreement with the observations by multiplying the theoretical amplitudes by the factor (0.65) needed to make the amplitude equal to the observed value (Fig. 10) at the Pribilof Islands. The one exception is the M2 amplitude east of St. Lawrence Island (NC17C) where the observed M2 amplitude remains larger than the model's.

The quantitative agreement (Table 5) is better for the three-dimensional model (Figs. 11 and 12) of Liu and Leenderste (1982, 1984). This may be due to the more complete dynamics in the three-dimensional model as well as the turning of this model to a larger set of tide observations than was available to Sündermann (1977). The simulation by Liu and Leenderste (1982, 1984) is for summer conditions without sea ice.

The new tidal observations should allow important improvements to be made in tidal models of the Eastern Bering Sea Shelf. One of these is the empirical model of Pearson *et al.* (1981). Unfortunately, the observations are still insufficient for an empirical model of the entire shelf because no observations are available near Cape Navarin and in the Gulf of Anadyr. Numerical models offer a way to fill this void.

At BC26, there is good agreement (Table 6) between the M2 current ellipse (Fig. 10) predicted by Sündermann (1977) and the observed ellipse

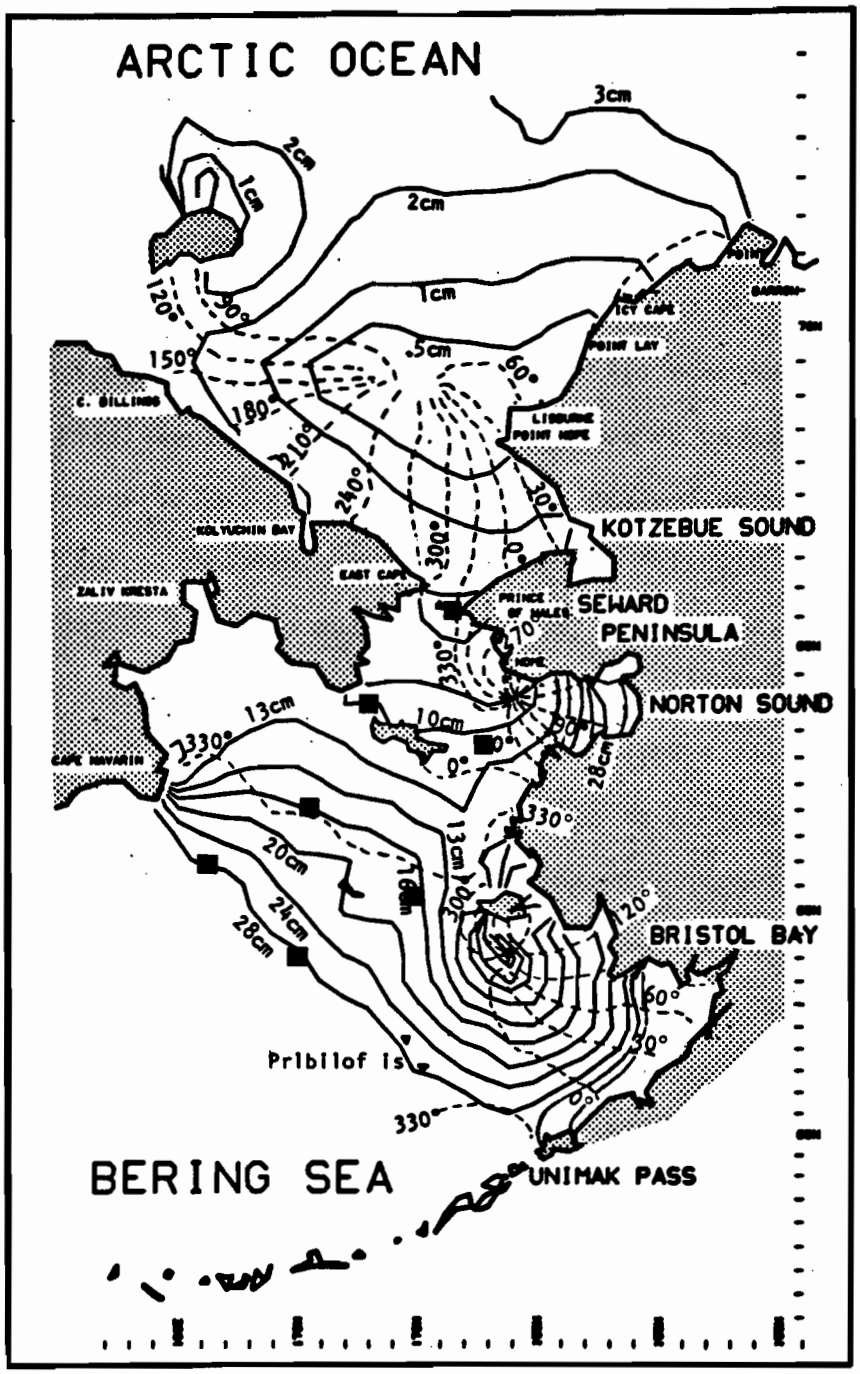

Figure 11. Composite diurnal tides in the Bering/Chukchi Sea from a three-dimensional model by Liu and Leenderste (1982, 1984). Also shown are locations (solid squares) of stations for which comparisons (Table 5) are made between the model and observations.

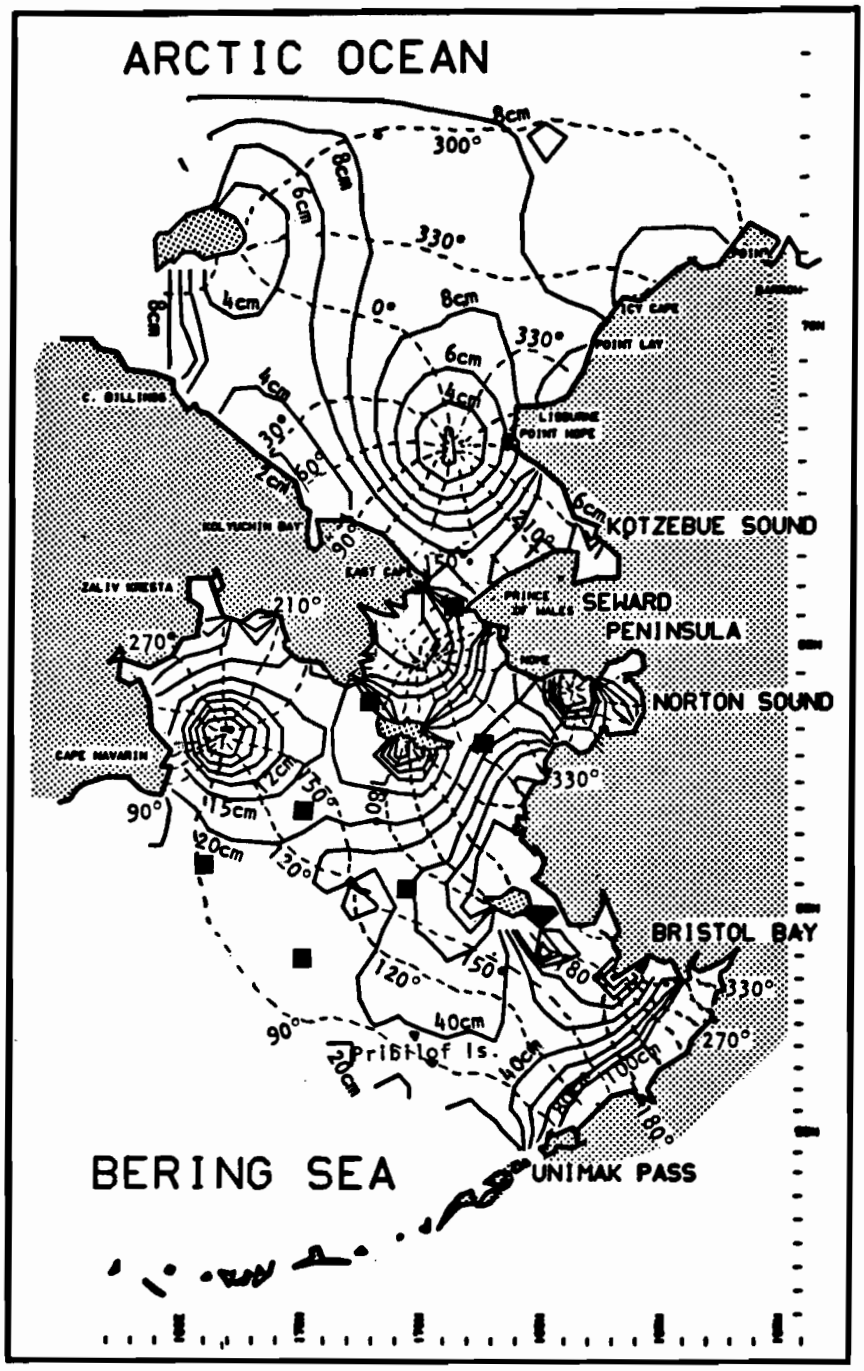

Figure 12. Composite semidiurnal tides in the Bering/Chukchi Sea from a three-dimensional model by Liu and Leenderste (1982, 1984). Also shown are locations (solid squares) of stations for which comparisons (Table 5) are made between the model and observations.

Table 6. Comparison of observed M2 current amplitudes with predicted values from the vertically integrated model by Sündermann (1977).

	Observed (cm/s)			Model (cm/s)		
	Major	Minor	Ratio	Major	Minor	Ratio
BC26	10.4	7.9	0.76	∿ 9.4	∿ 7.0	∿0.74
NC19B	5.3	0.6	0.11	∿12.6	∿ 3.6	∿0.29
NC25A	4.8	--	--	∿ 5.2	--	--
NC26A	3.1	1.1	0.35	∿ 6.2	∿ 3.2	∿0.52

(Table 3). In the vicinity of St. Lawrence Island (NC19B, NC25A and NC26A), the model (Table 6) predicts stronger M2 currents than those observed.

5. SUMMARY

Recent observations of tides and tidal currents on the Northeastern Bering Sea Shelf show that the diurnal tides dominate the tidal regime on the outer shelf. The diurnal tides decrease in amplitude inshore from the shelfbreak while the diurnal phase lags are nearly constant over a large region. The semidiurnal tides dominate the tidal regimes in Anadyr and Bering Straits.

The tides and tidal currents on the outer shelf show considerable resemblance to Sverdrup waves incident from the Aleutian Basin. The diurnal Sverdrup waves decrease rapidly in amplitude (evanescent) because their frequencies are less than the local Coriolis parameter. The semidiurnal tides and tidal currents agree less well with predictions based on Sverdrup waves, possibly because they are the superpositions of several waves associated with a semidiurnal amphidromic system off Cape Navarin.

There is good qualitative agreement of the tidal observations on the outer shelf with the predictions of a vertically integrated model by Sündermann (1977). The agreement is better with the preliminary results from a more recent, three-dimensional model by Liu and Leenderste (1982, 1984). Such models are essential for the construction of cotidal charts for the entire Eastern Bering Sea Shelf because there are no observations near Cape Navarin or in the Gulf of Anadyr available for the construction of empirical cotidal charts.

There are some seasonal variations in the tides and tidal currents on the Northeastern Bering Sea Shelf. The diurnal tides and tidal currents have a slight increase in amplitude during late winter while the diurnal phases are relatively constant, except for the larger phase lag of the diurnal tide in Bering Strait during the same period. The semidiurnal tide in Bering Strait and the semidiurnal currents near St. Lawrence Island decrease markedly in amplitude during late winter.

6. ACKNOWLEDGEMENTS

This memorandum is a contribution to the Marine Services Project of NOAA's Pacific Marine Environmental Laboratory. The pressure time series were obtained in cooperation with J. Schumacher and D. Pashinski, and the processing of these time series was carried out by P. Moen. Current time series were made available for this study by K. Aagaard, R. B. Tripp, and R. D. Muench. The author wishes to thank C. Pease, J. Schumacher and J. Overland for helpful discussions.

This study was funded in part by the Bureau of Land Management through an interagency agreement with the National Oceanic and Atmospheric Administration, under which a multiyear program is being conducted to respond to the need for petroleum development on the Alaskan Continental Shelf, and is managed by the Outer Continental Shelf Environmental Assessment Program (OCSEAP).

7. REFERENCES

Battisti, D.S., and A.J. Clarke (1982): A simple method for estimated barotropic tidal currents on continental margins with specific application to the M2 tide off the Atlantic and Pacific Coasts of the United States, *J. Phys. Oceanogr., 12*, 8-16.

Coachman, L.K., K. Aagaard, and R.B. Tripp (1975): *Bering Strait, The Regional Physical Oceanography*, University of Washington Press, Seattle, 172 pp.

Defant, A. (1961): *Physical Oceanography*, Volume 2, Pergamon Press, Oxford, 560 pp.

Fjeldstad, J.E. (1929): Contribution to the dynamics of free progressive tidal waves, Norwegian North Polar Exped. with the Maud, 1918-1925, Scientific Reports, Volume 4, 80 pp. (see Defant, 1961).

Harris, R.A. (1904): *Manual of Tides*, Part IV. Appendix 5, Report of Superintendent U.S. Coast and Geodetic Survey, Washington, D.C., 400 pp.

Kitani, K., and S. Kawasaki (1979): Oceanographic structure on the shelf edge region of the eastern Bering Sea - I: The movement and physical characteristics of water in summer, 1978, *Bull. Far Seas Fish. Res. Lab., 17*, 1-12 (in Japanese).

Leonov, A.K. (1960): *Regional Oceanography*, Part 1, Leningrad, 764 pp. (transl.).

Liu, S.-K., and J.J. Leenderste (1982): A three-dimensional shelf model of the Bering and Chukchi Seas, Amer. Soc. Civil Eng., *Coastal Engineering, 18*, 598-616.

Liu, S.-K, and J.J. Leenderste (1984): Modeling the Alaskan Coastal Waters, in Three-Dimensional Shelf Models (ed. by N. Heaps), *Amer. Geophys. Union*, Washington, D.C., in press.

Munk, W., F. Snodgrass, and M. Wimbush (1970): Tides off-shore: transition from California coastal to deep-sea waters, *Geophys. Fluid Dyn.*, *1*, 161-235.

Office of Climatology and Oceanographic Analysis Division (1961): *Climatological and Oceanographic Atlas for Mariners*, *2*, N. Pacific Ocean, 165 pp.

Pearson, C.A., H.O. Mofjeld, and R.B. Tripp (1981): Tides of the Eastern Bering Sea Shelf, in *The Eastern Bering Sea Shelf: Oceanography and Resources*, Volume 1 (ed. by D.W. Hood and J.A. Calder), U.S. Governmental Printing Office (dist. by University of Washington Press, Seattle), 111-130.

Salo, S.A., J.D. Schumacher, and L.K. Coachman (1983): Winter Currents on the Eastern Bering Sea Shelf, NOAA Technical Memorandum, ERL PMEL-45, 53 pp.

Sündermann, J. (1977): The semidiurnal principal lunar tide M2 in the Bering Sea, *Deutsche Hydro. Zeitschrift*, *30*, 91-101.

Sverdrup, H.U. (1927): Dynamics of tides on the North Siberian Shelf, *Geofis. Publ.*, *4*, 75 pp. (see Defant, 1961).